Click Here for Full Article

Estimation of incident photosynthetically active radiation from Moderate Resolution Imaging Spectrometer data

Shunlin Liang,[1] Tao Zheng,[1] Ronggao Liu,[2] Hongliang Fang,[1] Si-Chee Tsay,[3] and Steven Running[4]

[1] Incident photosynthetically active radiation (PAR) is a key variable needed by almost all terrestrial ecosystem models. Unfortunately, the current incident PAR products estimated from remotely sensed data at spatial and temporal resolutions are not sufficient for carbon cycle modeling and various applications. In this study, the authors develop a new method based on the look-up table approach for estimating instantaneous incident PAR from the polar-orbiting Moderate Resolution Imaging Spectrometer (MODIS) data. Since the top-of-atmosphere (TOA) radiance depends on both surface reflectance and atmospheric properties that largely determine the incident PAR, our first step is to estimate surface reflectance. The approach assumes known aerosol properties for the observations with minimum blue reflectance from a temporal window of each pixel. Their inverted surface reflectance is then interpolated to determine the surface reflectance of other observations. The second step is to calculate PAR by matching the computed TOA reflectance from the look-up table with the TOA values of the satellite observations. Both the direct and diffuse PAR components, as well as the total shortwave radiation, are determined in exactly the same fashion. The calculation of a daily average PAR value from one or two instantaneous PAR values is also explored. Ground measurements from seven FLUXNET sites are used for validating the algorithm. The results indicate that this approach can produce reasonable PAR product at 1 km resolution and is suitable for global applications, although more quantitative validation activities are still needed.

1. Introduction

[2] Terrestrial ecosystems are thought to be a major sink for carbon at the present time [*Houghton et al.*, 1998]. Different terrestrial ecosystem models, including models of terrestrial biogeochemistry [*Running and Gower*, 1991], global vegetation biogeography [*Prentice et al.*, 1992; *Prince*, 1991; *Prince and Goward*, 1995], dynamic vegetation [*Foley et al.*, 1996] and land-atmosphere exchange processes [*Bonan et al.*, 2002; *Dai et al.*, 2003; *Dickinson*, 1995; *Sellers et al.*, 1996], have been developed for the function and dynamic nature of ecosystems, along with their roles in the global carbon, nutrition, and water cycles. Almost all these models contain the physiological processes involved in photosynthesis and stomatal regulation that control the exchange of water vapor and carbon dioxide (CO_2) between vegetation canopies and the atmosphere. To initiate, calibrate and validate these models, various input data sets from various sources, particularly from remote sensing, are urgently required.

[3] Incident photosynthetically active radiation (PAR) is one such key input and is needed to model photosynthesis from single plant leaves to complex plant communities. The net primary production or the rate of carbon accumulation by terrestrial plant communities per unit area (C) is the difference of gross photosynthesis by the canopy (A_g) and autotrophic respiration of the stand (R):

$$C = A_g - R \tag{1}$$

To use remote sensing products as key inputs, the production efficiency models determine A_g at varied spatial scales [*Field et al.*, 1995; *Potter et al.*, 1993; *Prince and Goward*, 1995; *Running et al.*, 1999, 2000]:

$$A_g \propto \int e(t) \cdot fPAR(t) \cdot PAR(t)dt \tag{2}$$

where $e(t)$ is the radiation efficiency factor, *fPAR* represents the fraction of the *PAR* absorbed by green vegetation. A

[1]Department of Geography, University of Maryland, College Park, Maryland, USA.
[2]Institute for Geographical Science and Natural Resources Research, Chinese Academy of Sciences, Beijing, China.
[3]Climate and Radiation Branch, NASA/Goddard Space Flight Center, Greenbelt, Maryland, USA.
[4]School of Forestry, University of Montana, Missoula, Montana, USA.

number of process-based global NPP models do not explicitly calculate *fPAR*, but compute a leaf area index (LAI) [*Ruimy et al.*, 1999]. LAI and *fPAR* have a simple functional relationship. Monteith [*Monteith*, 1972, 1977] considered R to be a constant fraction of A_g, and, in such a case, spatial and temporal variations of C will be strongly determined by spatial and temporal variations of the absorbed PAR (APAR) (APAR = *fPAR* · *PAR*). *fPAR* is being produced by the MODIS (Moderate-Resolution Imaging Spectroradiometer) team as an Earth Observing System (EOS) standard product [*Myneni et al.*, 2002], but high-resolution incident *PAR* product over land simply does not exist although some efforts are being made [*Van Laake and Sanchez-Azofeifa*, 2004, 2005].

[4] A worldwide observation network for measuring incident PAR has not yet been established. The only practical means of obtaining incident PAR at spatial and temporal resolutions appropriate for most modeling applications is through remote sensing. Frouin and Pinker [*Frouin and Pinker*, 1995] reviewed the methods for estimating incident PAR from International Satellite Cloud Climatology Project (ISCCP) and Total Ozone Mapping Spectrometer (TOMS) observations. There have been two monthly ISCCP PAR products at 2.5° resolution. The ISCCP-BR PAR product was calculated from incident total shortwave flux divided by 2 [*Potter et al.*, 1993] using the ISCCP C1 data that are composed of both geostationary and polar-orbiter observations. The ISCCP-PL PAR product was derived from the PAR algorithm of Pinker and Laszlo [*Pinker and Laszlo*, 1992] also using the ISCCP C1 data. The TOMS PAR product was based on the method of Eck and Dye [*Eck and Dye*, 1991] using ultraviolet reflectivity. *Dye and Shibasaki* [1995] compared these three PAR products and found that ISCCP-BR and ISCCP-PL are typically 12–16% and 8–12% greater than TOMS PAR, respectively. Comparison of these three PAR products with ground data at a midlatitude site for nonwinter months by the same authors yielded the root mean square (RMS) differences of 28.1%, 13.7%, and 7.2%, and biases of +25.9%, +12.0%, and +2.8%, respectively.

[5] Because the high-resolution incident PAR over land surface is not a standard EOS product, the MODIS science team has to disaggregate the NASA data assimilation PAR product of 3-hourly 1° by 1.5° spatial resolution to produce 1 km NPP and net photosynthesis (PSN) products using the BIOME-BGC model [*Running et al.*, 1999, 2004]. The GLObal Production Efficiency Model (GLO-PEM) has to use 1° by 1° monthly TOMS PAR product for calculating global 8 km NPP product [*Prince and Goward*, 1995]. The TOMS PAR product is also limited to 66°N to 66°S latitude and is not available after 1989. The simplified PAR flux models are being used to produce the incident PAR flux over ocean from MODIS data [*Carder et al.*, 2003] and Sea-viewing Wide Field-of-View Sensor (SeaWiFS) data [*Frouin et al.*, 2000]. No PAR product has been routinely generated from MODIS or SeaWiFS over land. The incident PAR product constitutes a major uncertainty in carbon cycle modeling, and further developments are urgently needed.

[6] Satellite observations acquired at the top of the atmosphere (TOA) contain information of both atmosphere and surface. The current methods [e.g., *Carder et al.*, 2003; *Frouin et al.*, 2000; *Gu et al.*, 2004; *Pinker and Laszlo*, 1992; *Pinker et al.*, 2003] assume that either the atmospheric information is available from other sources (e.g., the ISCCP PAR product with atmospheric climatology data as input) or that water surface reflectances are known (e.g., SeaWiFS and MODIS PAR products over ocean).

[7] If the atmospheric parameters and surface spectral albedos are known, the existing algorithms [e.g., *Van Laake and Sanchez-Azofeifa*, 2004, 2005] may be directly applied. However, these models are based on the simple two-stream approximations for multiple scattering or even simpler schemes. Computation is speeded up significantly with the simplified models, but they usually are not accurate in calculating multiple scattering that dominates when the atmospheric optical depth is large (hazy or cloudy) and/or the surface is very bright (snow/ice). Simple models are easy to implement, and suitable for cases where no accurate input parameters are available (e.g., processing GOES data alone). Increasing the model complexity will increase difficulties of implementation for the regional and global applications. Instead, the look-up table approach is used in this study. It is specifically designed to achieve the high accuracy and keep a simple form of the model. The look-up table approach has been widely used in various scientific investigations.

[8] Another issue is the separation of direct and diffuse PAR radiation. The volume of shade within vegetation canopies is reduced by more than an order of magnitude on cloudy and/or very hazy days compared to clear, sunny days because of an increase in the diffuse fraction of the solar radiance. In a recent study, *Gu et al.* [2002] found that (1) diffuse radiation results in higher light use efficiencies by plant canopies; (2) diffuse radiation has much less tendency to cause canopy photosynthetic saturation; (3) the advantages of diffuse radiation over direct radiation increase with radiation level; and (4) temperature as well as vapor pressure deficit can cause different responses in diffuse and direct canopy photosynthesis, indicating that their impacts on terrestrial ecosystem carbon assimilation may depend on radiation regimes and thus sky conditions. These findings call for different treatments of diffuse and direct radiation in models of global primary production, and studies of the roles of clouds and aerosols in global carbon cycle [*Gu et al.*, 2003]. In fact, many land surface process models, such as SiB2 [*Sellers et al.*, 1996] and CLM [*Dai et al.*, 2003], have separated the direct and diffuse solar radiation. However, none of the existing PAR products separate these two components.

[9] In this study, the authors develop a new method for estimating incident PAR from MODIS data by estimating both surface and atmospheric information simultaneously. The key concept is the use of multitemporal signatures of MODIS data. Since the basic requirement of this method is the high temporal resolution, it potentially can be used for many different polar-orbiting sensors, such as Medium-Resolution Imaging Spectrometer (MERIS), SeaWIFS, Advanced Very High Resolution Radiometer (AVHRR), Global Land Imager (GLI) and Visible/Infrared Imager/Radiometer Suite (VIIRS), and geostationary sensors, such as geostationary operational environmental satellites (GOES).

[10] MODIS is one of the sensors in NASA's EOS Terra platform launched on 18 December 1999 for imaging in the

Table 1. A Typical Look-Up Table for Each Aerosol Model at a Specific Sun-Viewing Geometry, Where i = 1, 3, 4, v Denote MODIS Three Bands: 1 (Red), 3 (Blue), 4 (Green), and the Whole Visible Spectrum[a]

Visibility (Vi), km	$I_0^{(i)}$ i = 1, 3, 4	$F_d^{(i)}$ i = 1, 3, 4, v	$\gamma^{(i)}(\mu)$ i = 1, 3, 4	$\bar{\rho}^{(i)}$ i = 1, 3, 4, v
...	...	...	...	...
...	...	...	...	...

[a]Direct and diffuse PAR and total shortware radiations are three separate columns in the look-up table.

morning, and the Aqua platform launched on 4 May 2002 for imaging on the afternoon. MODIS has 36 spectral bands spanning from the visible to thermal-Infrared (IR) spectrum. The spatial resolution varies from 250 m (bands 1 and 2), 500 m (bands 3–7), to 1000 m (bands 8–36). The swath width of MODIS is about 2300 km, with the across-track field-of-view angle of 110°. Each MODIS sensor images the earth on a 2-day repeat cycle, with a 1-day or more frequent repeat at higher latitudes greater than 30° because of orbital convergence. The details of the sensor characterization are available elsewhere [*Salomonson et al.*, 1989].

[11] The details of the new method are presented in section 2. The validation results are shown in section 3. A series of related issues are discussed in section 4. A brief summary is given at the end of this paper.

2. New Method Description

[12] Incident PAR depends mainly on the atmospheric properties, but also to a lesser extent on surface reflectance. It can be demonstrated by the following formula for calculating downward spectral flux $F(\mu_0)$ at the solar zenith angle $\theta_0(\mu_0 = \cos(\theta_0))$ over a Lambertian surface [*Chandrasekhar*, 1960; *Liang*, 2004]:

$$F(\mu_0) = F_0(\mu_0) + \frac{r_s\bar{\rho}}{1 - r_s\bar{\rho}}\mu_0 E_0\gamma(\mu_0) \qquad (3)$$

where $F_0(\theta_0)$ is the downward flux without any contributions from the surface, r_s is surface reflectance, $\bar{\rho}$ is the spherical albedo of the atmosphere, E_0 is the extraterrestrial solar irradiance, $\gamma(\mu_0)$ is the total transmittance (direct plus diffuse) in the solar illumination direction. All radiometric variables are the function of wavelength. PAR is the integration of the downward spectral fluxes integrated from 400 nm to 700 nm:

$$PAR(\mu_0) = \int_{400}^{700} F_\lambda(\mu_0)d\lambda \qquad (4)$$

[13] We use the energy unit Wm^{-2} in our look-up tables. Note that many ecosystem process models typically employ PAR data in quantum units (photosynthetic photon flux density, $\mu mol\ m^{-2}s^{-2}$) and the conversion between the energy units to the quantum units was recently discussed by *Dye* [2004]. It is clear that the surface contribution to the incident PAR mainly depends on $r_s\bar{\rho}$. If the atmosphere is very clear (i.e., $\bar{\rho}$ is small) or the surface reflectance r_s is

low, the surface contribution to the incident PAR is relatively small.

[14] Our new method first estimates surface reflectance from multitemporal imagery and then PAR flux for each imagery. The basic procedure is composed of two steps, including (1) determination of the surface reflectance from the "clearest" observations during a temporal window and (2) calculation of incident PAR from the determined surface reflectance and TOA radiance/reflectance using the table look-up approach. Determining the length of the temporal window needs to be done carefully. Obviously, it must be short enough so the surface properties do not change dramatically, but long enough to include adequate clear observations. In all our case studies, it seems a period of one to three months is a reasonable choice. The details in each step are discussed below after introducing how to create look-up tables.

[15] Note that this new method differs from other methods in that surface reflectance and atmospheric properties are estimated simultaneously from imagery itself. For MODIS imagery, both aerosol/cloud optical depth and surface reflectance are the standard products from the MODIS science team. We can use these products for calculating PAR [e.g., *Van Laake and Sanchez-Azofeifa*, 2004, 2005]. However, some of these algorithms are not well developed at this point. For example, the aerosol optical depth products over land has many gaps (no retrieval) and is only available when the surface is densely vegetated [*Kaufman et al.*, 1997a, 1997b]. Besides, the MODIS atmospheric products have much coarser spatial resolution (~10 km). Therefore the method of Van Laake and Sanchez-Azofeifa is not suitable for estimating incident PAR from MODIS data at 1 km resolution.

2.1. Creating Look-Up Tables (LUT)

[16] For a Lambertian surface, the TOA upwelling radiance can be calculated from the classic formula [*Chandrasekhar*, 1960; *Liang*, 2004]:

$$I(\mu_0, \mu, \phi) = I_0(\mu_0, \mu, \phi) + \frac{r_s}{1 - r_s\bar{\rho}}\mu_0 E_0\gamma(-\mu_0)\gamma(\mu) \qquad (5)$$

where $I(\mu_0, \mu, \phi)$ is the observed TOA radiance at the viewing zenith angle θ, $\mu = \cos(\theta)$, and relative azimuth angle ϕ, $I_0(\mu_0, \mu, \phi)$ is path radiance without the surface contributions, and $\gamma(\mu)$ is the total transmittance from the surface to the sensor.

[17] Instead of online calculation of these atmospheric functions in equation (5) on the pixel basis that can be computationally very expensive, they are tabled offline as a function of aerosol or cloud optical depth at different viewing geometries. MODTRAN [*Berk et al.*, 1998] is used in this study, since it has been explored extensively in various simulations herein. In MODTRAN, multiple scattering is accurately calculated by DISORT [*Stamnes et al.*, 1988]. For each aerosol model at each specific sun-viewing geometry with a range of atmospheric visibility, three surface reflectance values are specified (0.0, 0.5 and 0.8) for the range of wavelengths at the interval of 15 wave numbers. MODTRAN outputs at each wavelength interval for these three surface reflectance are used to solve for $F_0(\mu_0)$, $F_d(\mu_0) = \mu_0 E_0\gamma(\mu_0)$, $\bar{\rho}$, $I_0(\mu_0, \mu, \phi)$, and $\gamma(\mu)$. These

Table 2. Cloud Extinction Coefficients (km^{-1}) at 0.55 μm, Thickness and Base Heights

	Altostratus Cloud	Stratus Cloud	Stratus/Stratocumulus Cloud	Nimbostratus Cloud
Extinction coefficients	1	1	1	1
Extinction coefficients	5	5	3	5
Extinction coefficients	20	15	10	10
Extinction coefficients	50	30	15	30
Extinction coefficients	128.1	56.9	38.7	45
Thickness, km	0.6	0.67	1.34	0.5
Base height, km	2.4	0.33	0.66	0.16

quantities are then integrated with the MODIS sensor spectral response functions over wavelength to get the average values for each wave band. The average values of $F_0(\mu_0)$, $F_d(\mu_0)$ and $\bar{\rho}$ over the visible spectrum (PAR region) also are calculated. Thus, for each aerosol model at a specific sun-viewing geometry (μ_0, μ, ϕ), there is a table that looks like Table 1. For clouds, the table looks the similar. Instead of changing visibility, cloud extinction values are changed.

[18] In this study, the following values have been used in the MODTRAN simulations: aerosol types (rural, maritime, urban and tropospheric), cloud types (altostratus, stratus, stratus/stratocumulus, and nimbostratus), solar zenith angle (0°, 20°, 40°, 50°, 60°, 65°, 70°, 75°, and 80°), viewing zenith angle (0°, 15°, 30°, 45°, and 65°), relative azimuth angle (0°, 30°, 60°, 90°, 120°, 150°, and 180°), and visibility for characterizing aerosol loadings (5, 10, 20, 30, 50 and 100 km). The default values of cloud thickness and base heights are used, but extinction coefficient varies for five values specified at 550 nm for each cloud type (see Table 2).

[19] The impacts of absorptive gases on incident PAR are examined through MODTRAN simulations. Because of their spatial and temporal variations, simulations are limited only to ozone and water vapor. The integrated transmittance of the PAR region at nadir and their concentrations are shown in Tables 3 and 4. By ignoring their variations, the uncertainty of the resulting PAR is clearly quite small. Therefore they are not considered as variables in the look-up tables.

[20] The look-up table approach is simple and fast, but has its limitations. It works only when the output is fairly linear with respect to changes in independent variables and the interactive effects of different variables are weak. It also limits the number of variables that can be considered in the simulation. The intervals of each variable in the look-up table need to be determined through a series of sensitivity studies so that a linear interpolation in the look-up table searching is valid.

2.2. Determination of Surface Reflectance

[21] The MODIS science team is routinely producing the land surface reflectance product routinely. One of its major inputs is the aerosol optical depth, which is estimated by using the "dark-object" method. The "dark-object" method has been widely used [*Liang*, 2004], but its limitation is that it is suitable only for dense vegetation canopies. In this study, we have developed a simpler method since incident PAR is much less dependant on surface reflectance.

[22] The central idea of this method is to detect the "clearest" observations in the temporal dimension for each pixel. Assuming that the aerosol optical depths for the "clearest" observation are known, its surface reflectance can be determined by assuming the surface is a Lambertian reflector. Surface reflectances of other "hazy/cloudy" observations are then interpolated from these "clearest" observations.

[23] The "clearest" observations are identified on the basis of their minimal blue band values. The underlying assumption is that when the atmosphere becomes more turbid, the blue band TOA radiance will be larger. On the other hand, surface reflectance at blue wavelengths is usually the lowest in the visible region [*Eck and Dye*, 1991]. Thus the blue band is a good choice for us to identify the "clear" atmospheric conditions. To avoid picking up the shadowing observations, we convert the TOA radiance of the blue band into the apparent surface reflectance from the look-up table values with a known aerosol visibility value for a very clear atmospheric condition (100 km is assumed in this study). If an observation contains cloud shadows, the converted surface reflectance value is usually negative and therefore flagged and excluded in determining surface reflectance. Here a fixed percentage of the total observations within the temporal window is used to determine the number of clear observations (e.g., 10%) at this stage. Ideally, it should be variable both spatially and temporally. More experiments may be needed in the future.

[24] As soon as the surface reflectance of these "clear" observations is calculated, the surface reflectance of other "hazy" observations can be linearly interpolated from them. To ensure that sufficient amount of "clear" observations are included in the temporal window, the length of the temporal window should be long enough. Thus surface reflectance within the temporal window may change and an interpolation process is necessary. In our experiments, it is found that the length of the temporal window of 1−3 months is reasonable.

Table 3. Ozone Concentration and the Integrated Transmittance Over the PAR Region

Concentration, gm/m^2	Transmittance
0.0	1.0
0.6393	0.9986
3.4804	0.9919
7.0319	0.9838
10.5833	0.9757
14.1347	0.9679
17.6862	0.9603

Table 4. Water Vapor Concentration and the Integrated Transmittance Over the PAR Region

Concentration, gm/m^2	Transmittance
0.0	1.0
0.3703	0.9993
2.0162	0.9957
4.0735	0.9919
6.1309	0.9885
6.7258	0.9875

[25] Although PAR flux is less dependant on surface reflectance, we need to consider an abrupt significant change of surface reflectance. The extreme case is the snowfall and snowmelt. The snow observations have to be labeled and separated from nonsnow observations. They must be processed separately but in the same fashion. The MODIS team is routinely producing snow and ice cover map. These maps can be used to distinguish snow and cloud, which has been an issue in previous studies [e.g., *Pinker et al.*, 2003]. What we do in this study is to group snow and nonsnow observations using the MODIS snow cover maps and apply the same procedures to these two groups separately.

2.3. Searching LUT for Calculating Incident PAR

[26] Given the surface reflectance from section 2.2 and TOA reflectance that is converted from digital numbers using the calibration coefficients, we can search the look-up tables and calculate incident PAR.

[27] For each pixel, if we know surface reflectance $r_s^{(i)}$, i = 1, 2, ... N, the TOA radiance $\hat{I}_j^{(i)}$ for these N bands can be predicted for each raw j in Table 1 using equation (5). The observed TOA radiance $I^{(i)}$ are then used to compare with $\hat{I}_j^{(i)}$ for determining the visibility value using linear interpolation since each j corresponds to one visibility value. The visibility value is the intermediate quantity and mainly used to interpolate other variables in the look-up tables. For each band (i), we can determine a visibility value. Because of the all possible uncertainties due to calibration and various assumptions, the resulting visibility values from different visible bands are usually different. Several schemes have been explored to calculate the PAR value.

[28] In scheme 1, for each estimated visibility value from each band, the downward flux of each band (F_i) is calculated by equation (3) with the quantities interpolated from Table 1 using the estimated visibility value. The PAR value is the linear combination of the spectral downward fluxes:

$$PAR = \alpha_0 + \sum_{i=1}^{N} \alpha_i F_i \qquad (6)$$

where α_i are the coefficients determined from simulations.

[29] In scheme 2, there is an estimated visibility value for each band, i, that is then used for interpolating the average values of several quantities ($F_0^{(v)}, \bar{\rho}^{(v)}, F_d^{(v)}$) from Table 1 so that PAR can be calculated in an aggregated fashion:

$$PAR^{(i)}(\mu_0) = F_0^{(v)}(\mu_0) + \frac{r_s^{(v)} \bar{\rho}^{(v)}}{1 - r_s^{(v)} \bar{\rho}^{(v)}} F_d^{(v)}(\mu_0) \qquad (7)$$

where the broadband visible reflectance $r_s^{(v)}$ is calculated from the spectral reflectance on the basis of our previous work [*Liang*, 2001, 2004]. For MODIS, the formula is

$$r_s^{(v)} = 0.331 r_s^{(1)} + 0.424 r_s^{(3)} + 0.246 r_s^4 \qquad (8)$$

Thus the final PAR value is the average value over these bands $\left(PAR = \frac{1}{N} \sum_{i=1}^{N} PAR^{(i)} \right)$.

[30] Scheme 3 is similar to scheme 2 except that the averaged visibility value is first calculated from all three bands and then the PAR is calculated using equation (7).

[31] Note that the direct, diffuse and total PAR are three columns in the look-up table, and each visibility value corresponds to these three quantities. As long as the visibility value is determined, they can be calculated in the same fashion.

3. Data Analysis

[32] In the following examples, we will demonstrate how the incident instantaneous PAR can be produced from MODIS data using this look-up table approach. In the first part, the validation results using ground measurements of seven stations of FLUXNET will be presented. The MODIS aerosol and cloud products are not used in these case studies, since the estimation of incident PAR is not very sensitive to the aerosol and cloud models. In the second part, mapping incident PAR over the greater Washington, D. C. region is presented to demonstrate that this method is suitable for regional and global applications.

3.1. Validation

[33] The validation experiments were conducted using ground measurements of incident PAR from seven FLUXNET sites: Black Hill, Fort Peck, Lost Creek, Howard forest (main tower), Oak Ridge, Sante Rem and Vaira Ranch. For each site, a 3 km * 3 km window (9 pixels) of the MODIS TOA radiance (MOD02) and angular values were extracted from the MODIS data sets ordered from the EOS gateway. The ground measurements collected every half-hour or 1 hour were compared with the retrieved values. The measurement values closest to the time of MODIS data acquisition were used to compare with the value of the central pixel in the extracted 9-pixel window without any interpolation. Because of the possible mismatch in both space and time, it is difficult to characterize the correlation between them using the traditional statistical analysis. Another mismatch problem is the amount of clouds and shadows existing in the different illumination and viewing paths. This effect is illustrated in Figure 1, showing the cloudy illumination path and clear viewing path (Figure 1a), and the clear illumination path but cloudy viewing path (Figure 1b). In the second case, the ground measured PAR could be much larger than the retrieved PAR from satellite observations even if the inversion is perfect. The ideal solution is to employ three-dimensional atmospheric radiative transfer modeling to account for all these factors. However, incorporating such a sophisticated radiative transfer calculation into the practical product generation continues to be a challenging topic in remote sensing.
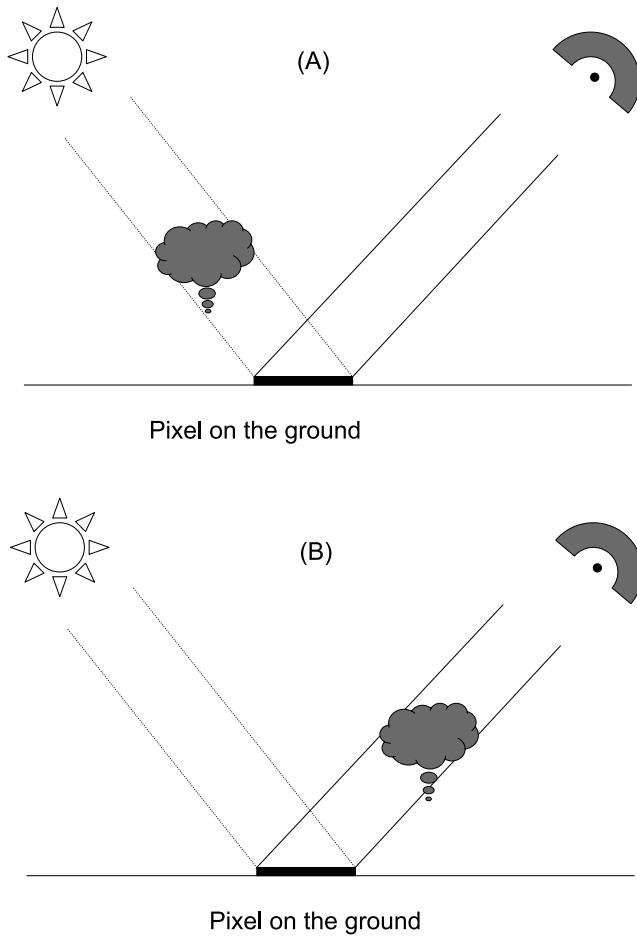
Figure 1. Illustrations of (a) the cloudy illumination path and clear viewing path and (b) the clear illumination path but cloudy viewing path.

[34] Instead, the statistics are determined using robust regression analysis technique, called the least trimmed squares (LTS) regression [*Rousseeuw*, 1984].This regression method minimizes the sum of the k smallest squared residuals (n/2 < k < n) where n is the number of data points. In this study, the largest squared residuals are trimmed by 10% (i.e., k/n = 0.9). The fitted statistics of all seven sites are summarized in Table 5a and shown in all validation figures. For comparison, the statistics from the ordinary regression analysis are summarized in Table 5b. In Table 5b, we also provide the mean relative error,

Table 5a. Summaries of Robust Regression Analysis at Seven Validation Sites

Sites	Intercept	Slope	Scale of the Residual	Robust Multipled R^2
Black Hills	−7.75	1.02	5.57	0.997
Fort Peck	3.57	1.00	36.33	0.996
Lost creek	2.39	1.00	19.15	0.999
Howard Forest	49.48	0.78	91.23	0.959
Oak Ridge	−0.03	1.00	0.79	1.000
Santa Rem	10.05	0.99	49.79	0.976
Vaira Ranch	−1.21	1.00	14.74	0.999

Table 5b. Summaries of Ordinary Regression Analysis at Seven Validation Sites

Sites	Intercept	Slope	Residual Standard Error	Multipled R^2	Average Relative Error, %
Black Hills	128.60	0.8645	116.6	0.9013	6.61
Fort Peck	193.13	0.8385	191.5	0.8804	15.1
Lost creek	66.801	0.9227	167.5	0.9247	10.2
Howard Forest	99.60	0.7394	161.8	0.8940	21.9
Oak Ridge	−3.513	1.0202	15.22	0.9881	4.1
Santa Rem	182.59	0.8195	136.9	0.8661	7.6
Vaira Ranch	12.523	0.9773	85.65	0.9788	4.2

defined as $\frac{1}{N}\sum_{i=1}^{N}\left|1-\frac{\hat{y}_i}{y_i}\right|$, where N is the total number of measurements, y_i and $\hat{y}_i$ are the observed and estimated PAR, respectively. The detailed analysis for each site is given below.
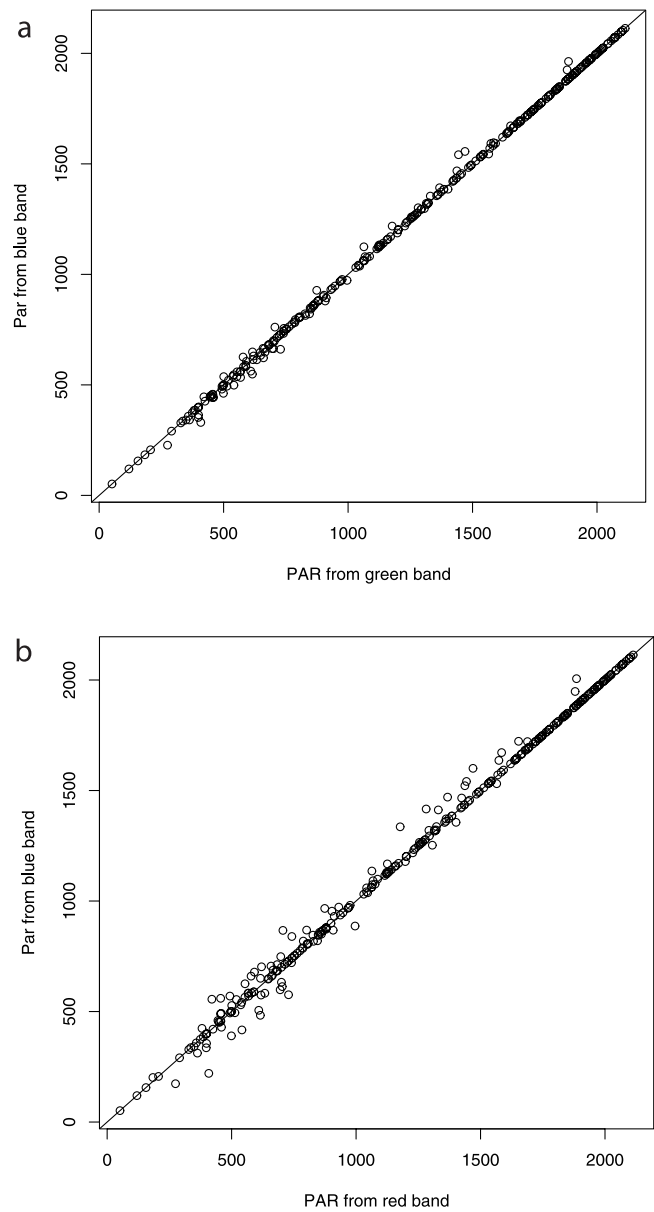

Figure 2. Comparisons of the retrieved PAR from three visible bands: (a) green and blue and (b) red and blue.
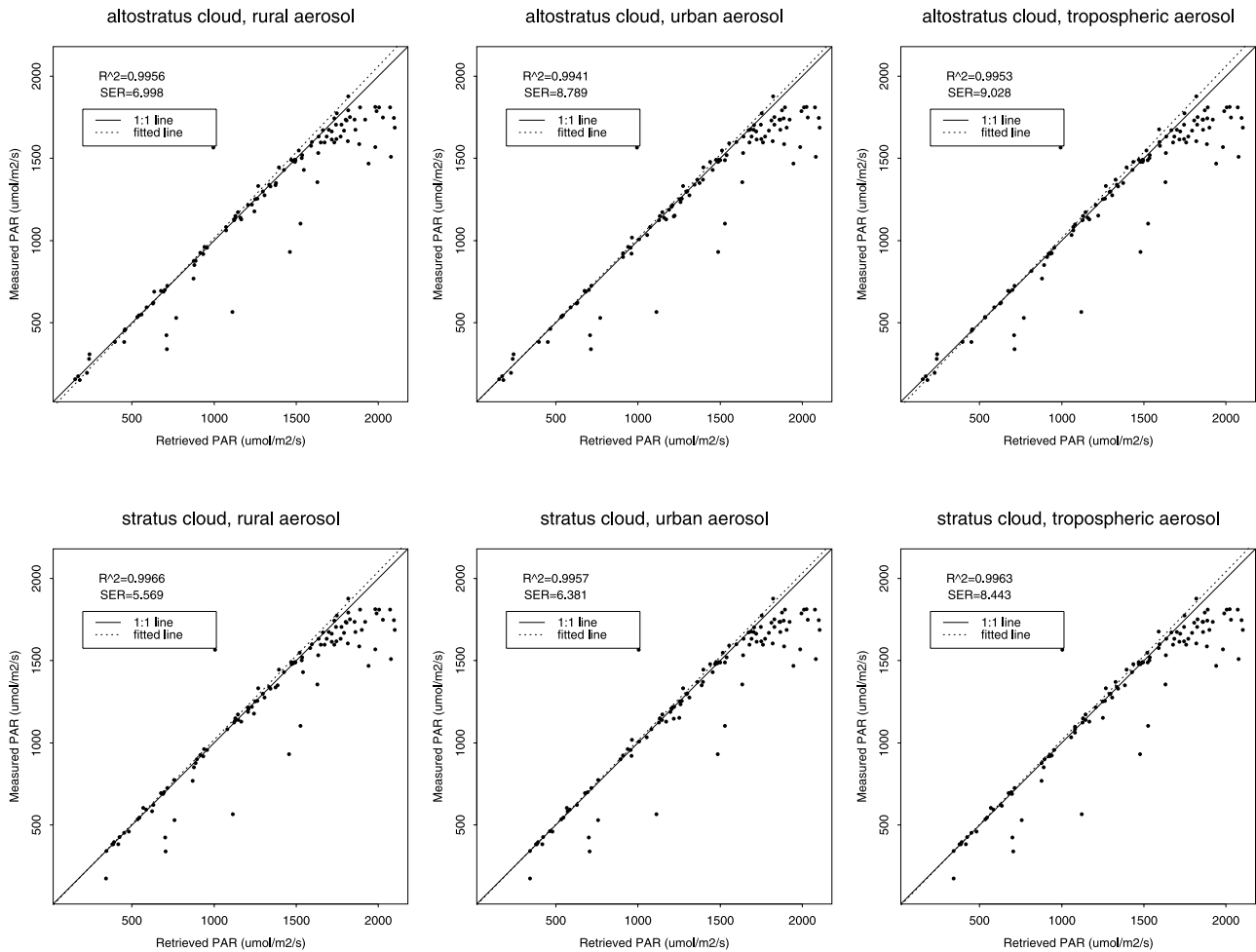
Figure 3. Comparisons of the retrieved incident PAR with three different aerosol types and two cloud types.

[35] The first site is Black Hill in North Dakota, which has an evergreen needleleaf forest and temperate landscape. The tower is located at 44°9′28.8″N, 103°39′W. The half-hour measurement data in 2002 from days 182–304 were used. Three schemes in searching the look-up tables are mentioned in section 1.3. Different schemes produce slightly different retrievals, but the differences are quite small. We prefer to scheme 2. Further data analysis indicate that using even only one band is sufficient to produce the PAR, instead of the average estimates from all three bands, since the retrievals from all three bands are very similar (see Figure 2). These assessments can reduce the computation time and space requirement significantly. Finally, the blue band (band 3) is selected in this study.

[36] It was also found that selecting different cloud types and aerosol types does not significantly affect the PAR retrieval. Figure 3 shows the results of three different aerosol types and two cloud types. Determining the aerosol and cloud types from MODIS data is still very challenging. Given the relative small differences, rural aerosol and stratus cloud are used in the rest of the paper.

[37] The second site is the Fort Peck (48°18.473′N and 105°6.032′W), Montana station, located on the Fort Peck Tribes Reservation, approximately fifteen miles north of
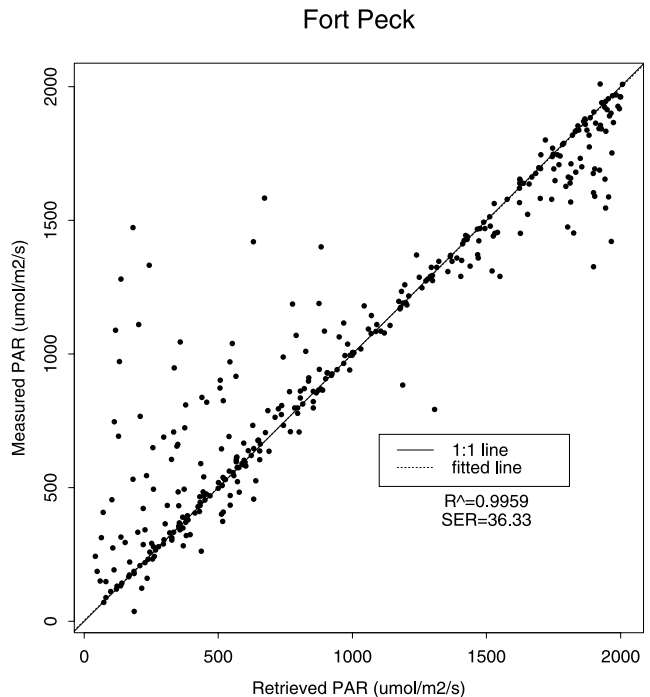

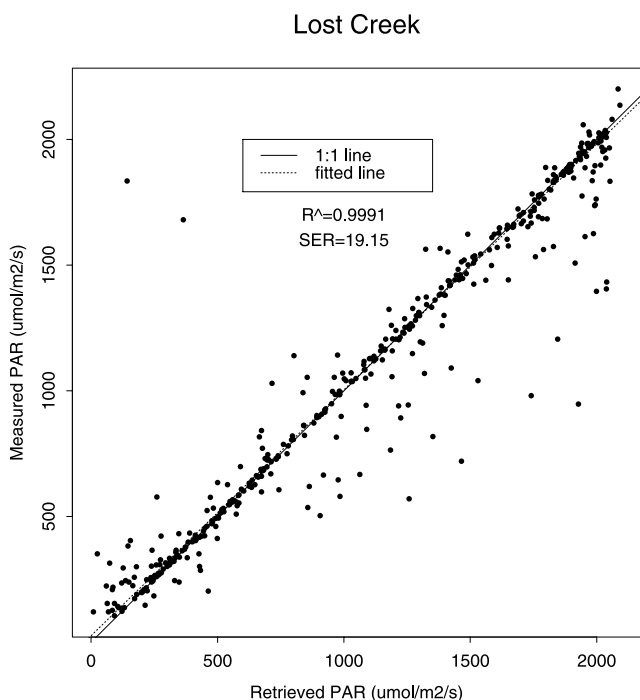**Figure 4.** Validation results at FLUXNET site Fort Peck.

Lost Creek

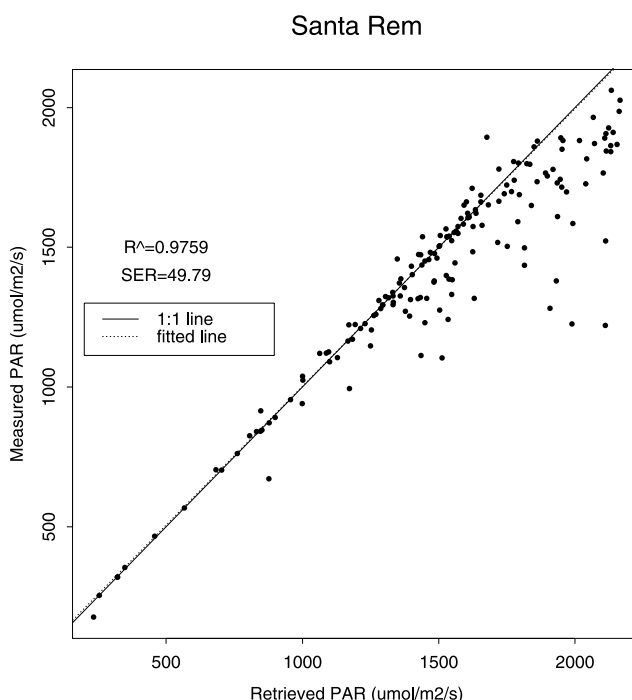**Figure 5.** Validation results at FLUXNET site Lost Creek.

Main Tower

Figure 6. Validation results at FLUXNET site Main Tower.

Poplar, Montana. A tower of 3 m high was installed in November of 1999 over grassland with a surface elevation of 634 m. The comparison of the retrieved and measured half-hour incident PAR in 2002 (the whole year) is shown in Figure 4. The overall fitting is very good, although there are some pixels of overestimation with high PAR values and underestimation with low PAR values.

Santa Rem

Figure 7. Validation results at FLUXNET site Santa Rem.

[38] Note that all measurements are in the unit of μmol/m²/s, but our look-up table PAR outputs are in Wm^{-2}. For quick comparisons, we simply used the conversion factor 4.6. However, the conversion factor is supposed to vary under different conditions (see *Dye* [2004] for details).

[39] The third site is Lost Creek, (46°4.9′N, 89°58.7′W), located in northern Wisconsin. The elevation is about 480 m above sea level. The biome is mixed forest with canopy height of 1−2 m. This site was established on 4 September 2000. The measurement data from both 2000 and 2001 were used here and the validation results are shown in Figure 5. The fitting is better than the two previous sites.

[40] The fourth site is Howland forest (Main Tower), located at Howland, Maine (45.204°N, 68.74°W). Topographically, the region varies from flat to gently rolling with a maximum elevation change of less than 68 m, The landscape is composed of a deciduous evergreen needle forest, boreal/northern hardwood, old coniferous, hemlock, douglas fir, and evergeen coniferous. It is chiefly cold, temperate and humid. The region is covered by the snow of up to 2 m from December through March. Measurement data in 2002 from dates 74−365 were downloaded. The validation results are shown in Figure 6, which are the worst in all cases since the retrievals are biased. We had difficulty in figuring out what causes this bias, which is not obvious in other sites. The instrument calibration could be a factor, but we are making efforts to intercompare the PAR products from other sensors.

[41] The fifth site is the Tapajos National Forest (Santa Rem − Km83) over the logged evergreen tropical broadleaf forest at Brazil. The geographic coordinates of the tower is 3°1′4.9″S, 54°58′17.166″W. The measured PAR data started from 1999, but only data in 2001 were used in this study. The comparison is shown in Figure 7. The overall validation results are good, although there exist some pixels of
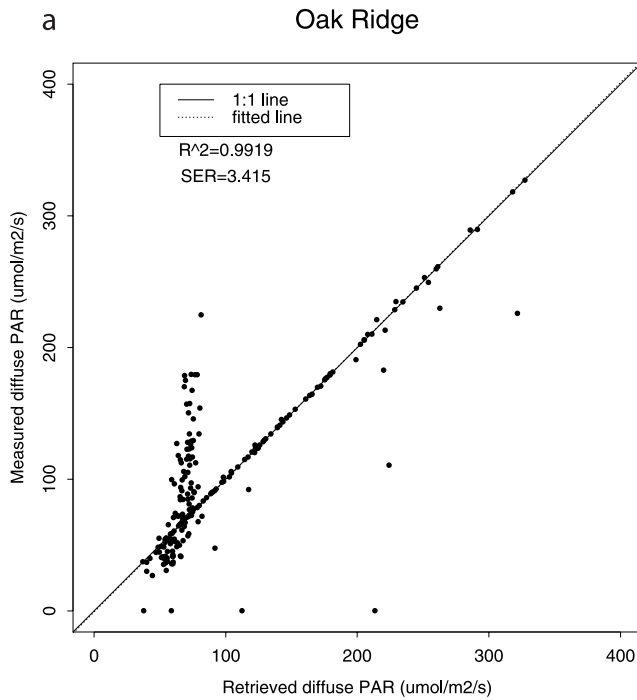
a

Oak Ridge

Figure 8. Validation results at FLUXNET site Oak Ridge: (a) diffuse, (b) direct, and (c) total PAR.

c

Oak Ridge

Figure 8. (continued)

overestimation when the PAR values are large. Since this site is in the tropic region, broken clouds and rapid movements of cloud could be a contributing factor.

[42] The sixth site is the Walker Branch Watershed (35°57′31.56″N, 84°17′14.76″W), located at Oak Ridge, Tennessee. It has a forest stand over 50 years old, having regenerated from agricultural land. It has a temperate climate, with a mixed species, broad-leaved forest, deciduous forest, oak and hickory. This site is the only one where both direct and diffuse radiation values are measured. The validation results are shown in Figure 8. The direct component has a much larger scatter, including a group of underestimation pixels, but the agreements for the diffuse and the total PAR appear much better. Because of the spatial
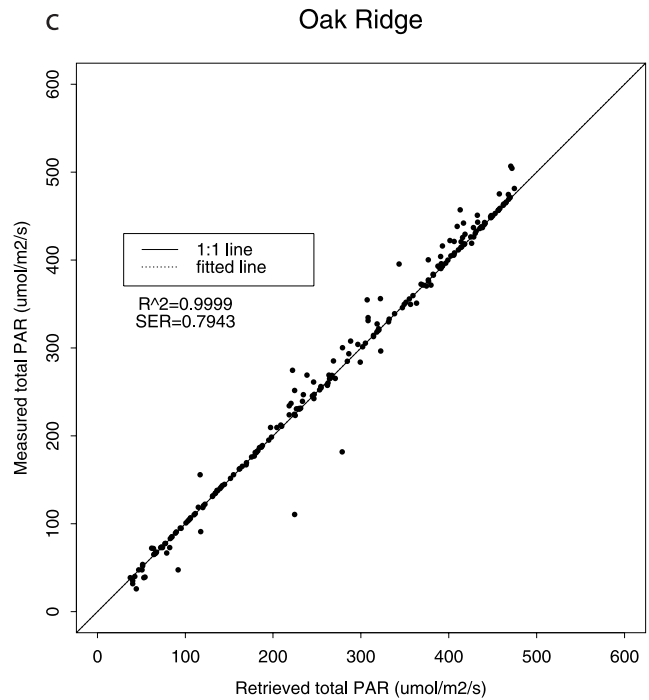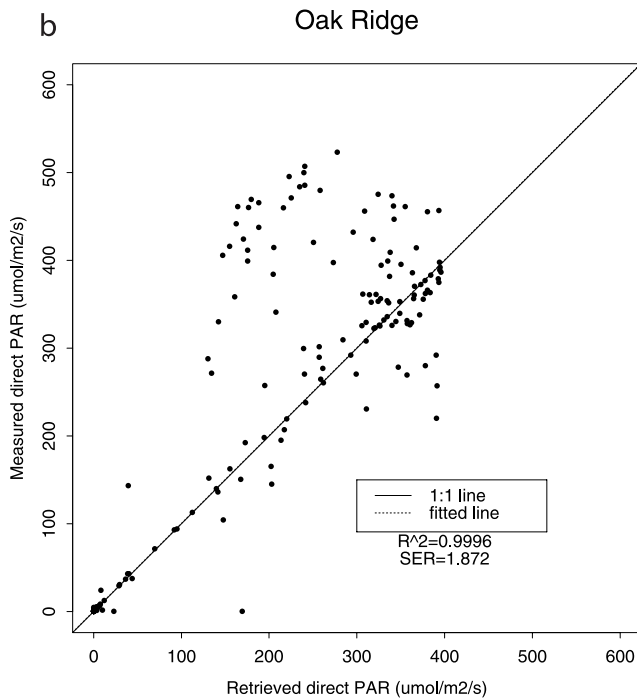
b

Oak Ridge

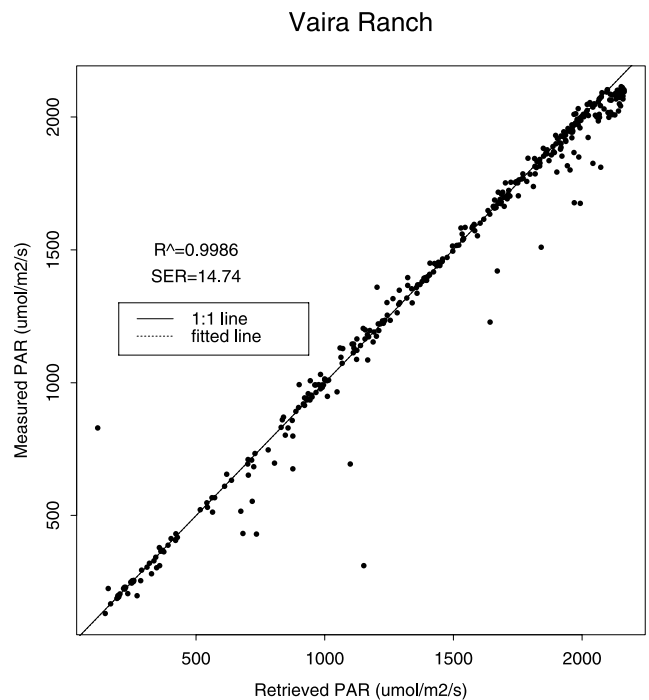
Figure 8. (continued)

Vaira Ranch

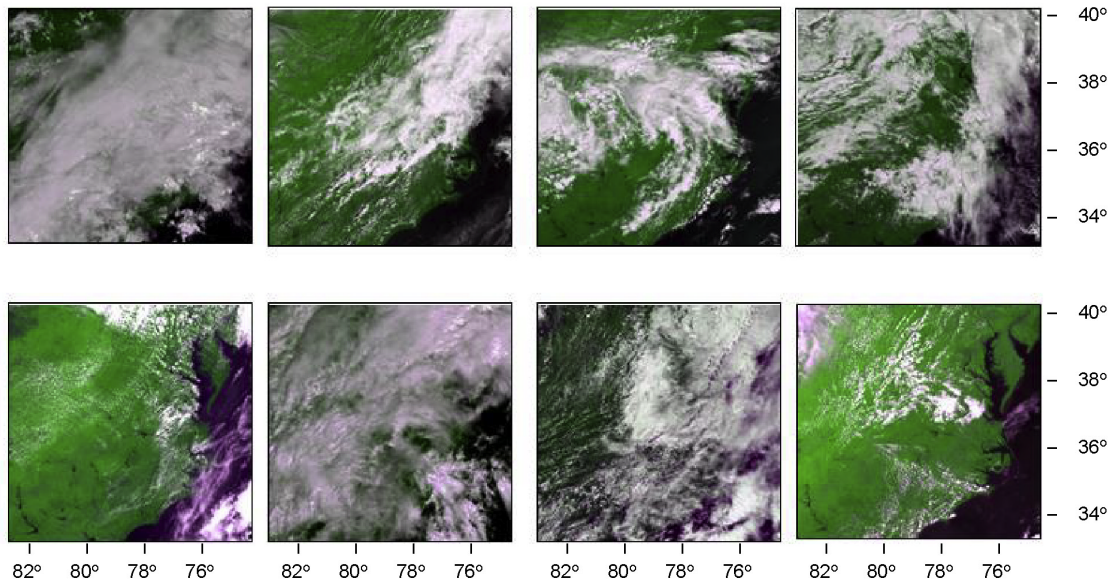**Figure 9.** Validation results at FLUXNET site Vaira Ranch.

Figure 10. True color composite MODIS imagery of greater Washington, D. C., area in 8 days (22 May, 25 May, 29 May, 31 May, 5 June, 7 June, 8 June, and 10 June 2003).

and temporal mismatch between the ground measurements and MODIS data, the large difference of the direct component is not surprising. In the future validation, we ought to investigate whether the inversion method also contributes to the differences. For example, the direct PAR may be very sensitive to the existence of partial clouds, while our method assumes plane-parallel atmospheric properties. Another factor could be the conversion constant that coverts the energy unit in our code to the quantum unit in the measurement. We used a constant, but it could be variable [*Dye*, 2004].

[43] The last site is the Vaira Ranch (38°24.4′N and 120°57.044′W) at Ione, California, situated in a topograph-

ically undulating oak and grass savanna biome in eastern California at the foot of the Sierra Nevada Mountains. The surrounding landscape is grazed grass rangeland. The elevation at the tower location is 129 m. A year of half-hour measurements in 2002 was used in this study. The fitted results are shown in Figure 9, and the agreement is excellent.

[44] It is clear that this method can produce reasonably accurate incident PAR products from MODIS observations. However, there are large scatters in some cases. The spatial and temporal mismatches between the ground "point" measurements and the MODIS pixel values are probably the major source of these differences. Other factors
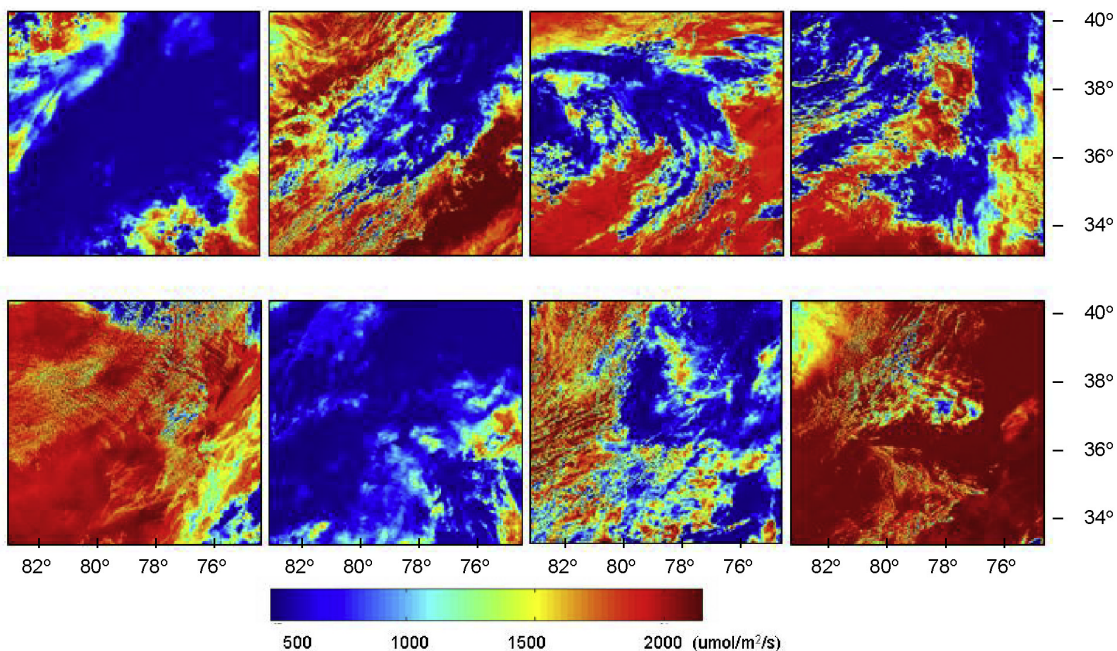

Figure 11. Retrieved incident PAR maps from the corresponding MODIS images in Figure 10.

may include the plane-parallel atmospheric radiative transfer model that is used for creating the look-up tables but fails to account for broken clouds in the atmosphere, surface Lambertian assumption, linear interpolation in table searching, uncertainty in determining surface reflectance, and so on.

3.2. Mapping INCIDENT PAR Over the Greater Washington, D. C. Area

[45] To test the method for the regional mapping, the incident PAR over the greater Washington, DC area was mapped in 2003. It is impractical to show all these images here and the estimated PAR maps; instead, the images of the following 8 days (142, 145, 149, 151, 156, 158, 159, and 161) are presented in this paper with variable atmospheric conditions and visual spatial patterns. The true color composite images (using bands 1,3 and 4) are shown in Figure 10, and the estimated corresponding incident PAR maps are shown in Figure 11. The image dimension is 800 by 800 pixels. It is clear there are very good correlations between the original image, and the mapped PAR and the patterns match very well.

4. Calculating Daily PAR

[46] Instantaneous PAR can be very useful to NPP and other ecosystem models. However, many models have the daily time step and thus the daily PAR product is more desirable. If the high-frequency data from a geostationary satellite (e.g., GOES) are available, calculating daily values would be easier. An alternative method is explored in this study.

[47] The daily PAR is calculated from two instantaneous PAR products (MODIS/Terra (AM) and MODIS/Aqua (PM). Experiments show that the diurnal cycle can be approximated by cosine function of the local solar zenith angle [e.g., *Tarpley*, 1979]. Following the same logic, the morning and afternoon diurnal cycles are expressed by two different functions. Specifically, MODIS/Terra instantaneous PAR values are used for determining the coefficient of the morning function, and MODIS/Aqua instantaneous PAR values are used for determining the afternoon function. The daily PAR is simply the integration of these two functions. The simpler version of this method is to conduct the regression between MODIS-estimated instantaneous values and the daily average.

[48] After analyzing these ground measurement data (section 3.1), it was found the predicted daily mean PAR flux, using one or two instantaneous MODIS PAR fluxes, can be reasonably accurate. Figure 12 shows the fitting results using in situ data of these FLUXNET sites. The corresponding equations for calculating the daily 24-hour average PAR from one morning PAR at 1030 local time (LT) (PAR_{am}) or one afternoon PAR (PAR_{pm}) at 1330 LT or both:

There is a high degree of variation. Note that in the high latitude regions there are multiple MODIS observations each day from which the daily average values will be predicted more accurately.

5. Incident PAR and Shortwave Insolation

[49] Since direct measurement of incident PAR is just beginning and is still quite limited in space, it has been assumed in various applications that incident PAR is half of the incident shortwave radiation (insolation) that has routinely been measured by weather stations. Several studies have indicated that this ratio is not a constant. *Jacovides et al.* [2003] found that this ratio varies from 0.460 to 0.501 from the hourly measured values.

[50] *Alados et al.* [1996] found that this ratio also has seasonal and daily variations. The ratio is smaller and more variable in winter than in summer, and is usually low at noon.

[51] On the other hand, the total shortwave radiation is also required by any land surface process models and many other applications. Using our new method, the total shortwave downward flux can be organized in the same look-up tables as incident PAR. Thus they can be determined simultaneously. The surface reflectance of broadband total shortwave can be converted from narrowband reflectance using the formula developed earlier [*Liang*, 2001].

6. Summary

[52] High resolution incident PAR over land is needed by ecological and hydrological modeling, but has not been routinely generated from satellite observations. A new method for estimating incident PAR from MODIS imagery using the look-up table method has been presented above. The unique feature of this new method is that both surface reflectance and atmospheric properties are estimated simultaneously, while most existing algorithms require ancillary information from other sources about aerosols and clouds. The use of the look-up table also can enable us to avoid use of the two-stream approximations in calculating multiple scattering as used in most current algorithms since they may result in significant errors. The table search is also very expedient, so this method can be easily implemented for regional and global applications. Its limitation is that it cannot include many input variables. The linear interpolation in the table search may introduce errors particularly when the intervals in the table are large.

[53] The surface reflectances are estimated from the temporal signatures using the minimum blue reflectance. The look-up tables are established by using the MODTRAN radiative transfer package. The method can separate direct and diffuse components of incident PAR, and the total

$$
\begin{cases}
PAR\_daily = 39.86 + 0.0784 * PAR_{am} + 1.5277 * 10^{-4} * PAR_{am}^2 \\
\\
PAR\_daily = -6.637 + 0.3571 * PAR_{pm} \\
\\
PAR\_daily = 29.7 + 0.0129 * PAR_{am} + 1.1715 * 10^{-4} * PAR_{am}^2 + 0.128 PAR_{pm}
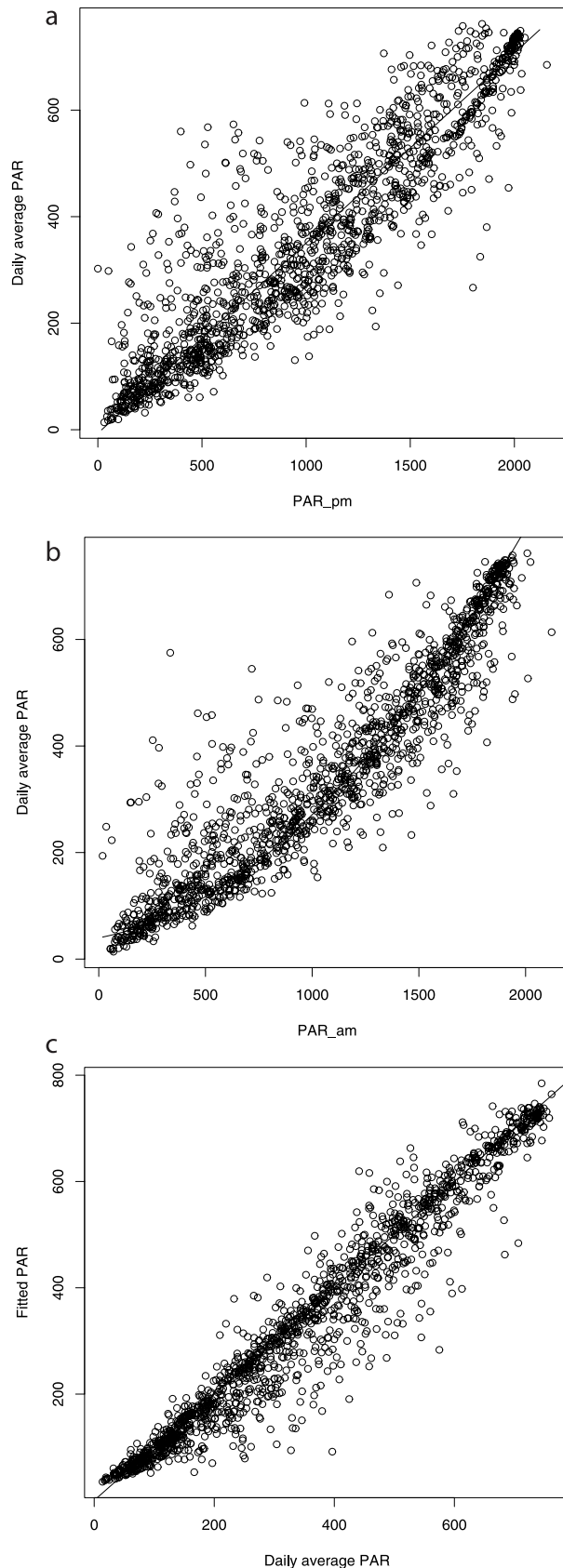\end{cases}
\tag{9}
$$

Figure 12. Predicting daily average PAR from one or two simultaneous PAR at MODIS overpass times using (a) one afternoon MODIS PAR, (b) one morning MODIS PAR, and (c) both.

shortwave radiative flux (insolation) can be also determined from the same look-up table.

[54] The method has been validated using FLUXNET observations from seven stations. The validation results indicate that this method is reasonably accurate. Although more validation activities are on the way, we feel confident at this point that this method is very reliable for mapping incident PAR from MODIS data.

[55] Because of the importance of diffuse PAR in modeling and other applications, validating the diffuse PAR product is critical. However, such ground measurements are rare. Greater efforts should be made to measure diffuse PAR component in the current or future observation networks.

[56] MODIS estimates of incident PAR are instantaneous; the ideas for calculating daily averages are also discussed. The current algorithms for generating PAR products have not usually considered topography. This issue is particularly relevant for carbon cycle modeling when the spatial resolution increases, since most forests are distributed over the mountainous regions. These issues will be addressed in the future. We plan to evaluate the impacts of the improved incident PAR product on the MODIS GPP/NPP products, and distribute this product through the University of Maryland Global Land Lover Facilities.

References

Alados, I., I. Foyo-Moreno, and L. Alados-Arboledas (1996), Photosynthetically active radiation: measurements and modelling, *Agric. For. Meteorol.*, *78*, 121–131.

Berk, A., L. S. Bernstein, G. P. Anderson, P. K. Acharya, D. C. Robertson, J. H. Chetwynd, and S. M. Adler-Golden (1998), MODTRAN cloud and multiple scattering upgrades with application to AVIRIS, *Remote Sens. Environ.*, *65*, 367–375.

Bonan, G. B., K. W. Oleson, M. Vertenstein, S. Levis, X. Zeng, Y. Dai, R. E. Dickinson, and Z. L. Yang (2002), The land surface climatology of the community land model coupled to the NCAR community climate model, *J. Clim.*, *15*, 3123–3149.

Carder, K., R. Chen, and S. Hawes (2003), Instantaneous photosynthetically available radiation and absorbed radiation by phytoplankton, MODIS Ocean Science Team Algorithm Theoretical Basis Document, ATBD MOD-20, version 7, 24 pp., NASA Goddard Space Flight Cent., Greenbelt, Md., Feb. (Available at http://modis.gsfc.nasa.gov/data/atbd/ocean_atbd.php).

Chandrasekhar, S. (1960), *Radiative Transfer*, Dover, Mineola, N. Y.

Dai, Y., et al. (2003), The Common Land Model (CLM), *Bull. Am. Meteorol. Soc.*, *84*(8), 1013–1023.

Dickinson, R. E. (1995), Land-atmosphere interaction, *Rev. Geophys*, *33*(S1), 917–922.

Dye, D. (2004), Spectral composition and quanta-to-energy ratio of diffuse photosynthetically active radiation under diverse cloud conditions, *J. Geophys. Res.*, *109*, D10203, doi:10.1029/2003JD004251.

Dye, D. G., and R. Shibasaki (1995), Intercomparison of global PAR data sets, *Geophys. Res. Lett.*, *22*, 2013–2016.

Eck, T. F., and D. G. Dye (1991), Satellite estimation of incident photosynthetically active radiation using ultraviolet reflectance, *Remote Sens. Environ.*, *38*, 135–146.

Field, C. B., J. T. Randerson, and C. M. Malmstrom (1995), Global net primary production: Combining ecology and remote sensing, *Remote Sens. Environ.*, *51*, 74–88.

Foley, J. A., I. C. Prentice, N. Ramunkutty, S. Levis, D. Pollard, S. Sitch, and A. Haxeltine (1996), An integrated biosphere model of land surface

processes, terrestrial biosphere model of ecosystem dynamics, *Global Biogeochem. Cycles*, 10, 603–628.

Frouin, R., and R. Pinker (1995), Estimating photosynthetically active radiation (PAR) at the Earth's surface from satellite observations, *Remote Sens. Environ.*, 51, 98–107.

Frouin, R., B. Franz, and M. Wang (2000), Algorithm to estimate PAR from SeaWiFS data, NASA SeaWiFS technical report, version 1.2, 15 pp., NASA Goddard Space Flight Cent., Greenbelt, Md. (Available at http://daac.gsfc.nasa.gov/oceancolor/documentation/OB_Documentation.shtml).

Gu, L., D. Baldocchi, S. B. Verma, T. A. Black, T. Vesala, E. M. Falge, and P. R. Dowty (2002), Advantages of diffuse radiation for terrestrial ecosystem productivity, *J. Geophys. Res.*, 107(D6), 4050, doi:10.1029/2001JD001242.

Gu, L. H., D. D. Baldocchi, S. C. Wofsy, J. W. Munger, J. J. Michalsky, S. P. Urbanski, and T. A. Boden (2003), Response of a deciduous forest to the Mount Pinatubo eruption: Enhanced photosynthesis, *Science*, 299(5615), 2035–2038.

Gu, J., et al. (2004), Modeling carbon sequestration over the large-scale Amazon basin, aided by satellite observations. Part I: Wet- and dry-season surface radiation budget flux and precipitation variability based on GOES retrievals, *J. Appl. Meteorol.*, 43, 870–886.

Houghton, R. A., E. A. Davidson, and G. M. Woodwell (1998), Missing sinks, feedbacks, and understanding the role of terrestrial ecosystems in the global carbon balance, *Global Biogeochem. Cycles*, 12(1), 25–34.

Jacovides, C. P., F. S. Tymvios, D. N. Asimakopoulos, K. M. Theofilou, and S. Pashiardes (2003), Global photosynthetically active radiation and its relationship with global solar radiation in the eastern Mediterranean basin, *Theor. Appl. Climatol.*, 74(3–4), 227–233.

Kaufman, Y. J., D. Tanré, L. Remer, E. F. Vermote, A. Chu, and B. N. Holben (1997a), Operational remote sensing of tropospheric aerosol over the land from EOS-MODIS., *J. Geophys. Res.*, 102(D14), 17,051–17,068.

Kaufman, Y. J., A. Wald, L. A. Lorraine, B. C. Gao, R. R. Li, and L. Flynn (1997b), Remote sensing of aerosol over the continents with the aid of a 2.2 um channel, *IEEE Trans. Geosci. Remote Sens.*, 35, 1286–1298.

Liang, S. (2001), Narrowband to broadband conversions of land surface albedo, *Remote Sens. Environ.*, 76, 213–238.

Liang, S. (2004), *Quantitative Remote Sensing of Land Surfaces*, 534 pp., John Wiley, Hoboken, N. J.

Monteith, J. L. (1972), Solar radiation and productivity in tropical ecosystems, *J. Appl. Ecol.*, 9, 747–766.

Monteith, J. L. (1977), Climate and the efficiency of crop production in Britain, *Philos. Trans. R. Soc. London, Ser. B*, 281, 277–294.

Myneni, R. B., et al. (2002), Global products of vegetation leaf area and fraction absorbed PAR from year one of MODIS data, *Remote Sens. Environ.*, 83(1–2), 214–231.

Pinker, R. T., and I. Laszlo (1992), Modeling surface solar irradiance for satellite applications on a global scale, *J. Appl. Meteorol.*, 31, 194–211.

Pinker, R. T., et al. (2003), Surface radiation budgets in support of the GEWEX Continental-Scale International Project (GCIP) and the GEWEX Americas Prediction Project (GAPP), including the North American Land Data Assimilation System (NLDAS) project, *J. Geophys. Res.*, 108(D22), 8844, doi:10.1029/2002JD003301.

Potter, C. S., et al. (1993), Terrestrial ecosystem production: a process model based on global satellite and surface data, *Global Biogeochem. Cycles*, 7, 811–841.

Prentice, I. C., W. Cramer, S. P. Harrison, R. Leemans, R. A. Monserud, and A. M. Solomon (1992), A global biome model based on plant physiology and dominance, soil properties and climate, *J. Biogeogr.*, 19, 117–134.

Prince, S. D. (1991), A model of regional primary production for use with coarse resolution satellite data, *Int. J. Remote Sens.*, 12, 1313–1330.

Prince, S. D., and S. N. Goward (1995), Global primary production: a remote sensing approach, *J. Biogeogr.*, 22(4–5), 815–835.

Rousseeuw, P. J. (1984), Least median of squares regression, *J. Am. Stat. Assoc.*, 79, 871–881.

Ruimy, A., L. Kergoat, and A. Bondeau (1999), Comparing global models of terrestrial net primary productivity (NPP): Analysis of differences in light absorption and light-use efficiency, *Global Change Biol.*, 5, 56–64.

Running, S., and S. T. Gower (1991), Forest-BGC, a general model of forest ecosystem processes for regional applications, II. Dynamic allocation and nitrogen budgets, *Tree Physiol.*, 9, 147–160.

Running, S. W., R. Nemani, J. M. Glassy, and P. Thornton (1999), MODIS daily photosynthesis (PSN) and annual net primary production (NPP) product (MOD17), MODIS Land Science Team Algorithm Theoretical Basis Document (ATBD), ATBD-MOD16, version 3.0, 59 pp., NASA Goddard Space Flight Cent., Greenbelt, Md., 29 Apr. (Available at http://modis.gsfc.nasa.gov/data/atbd/land_atbd.php).

Running, S. W., P. E. Thornton, R. Nemani, and J. M. Glassy (2000), Global terrestrial gross and net primary productivity from the Earth Observing System, in *Methods in Ecosystem Science*, edited by O. E. Sala et al., pp. 44–57, Springer, New York.

Running, S. W., R. R. Nemani, F. A. Heinsch, M. S. Zhao, M. Reeves, and H. Hashimoto (2004), A continuous satellite-derived measure of global terrestrial primary production, *Bioscience*, 54(6), 547–560.

Salomonson, V., W. Barnes, P. Maymon, H. Montgomery, and H. Ostrow (1989), MODIS: Advanced facility instrument for studies of the Earth as a system, *IEEE Trans. Geosci. Remote Sens.*, 27, 145–153.

Sellers, P. J., S. O. Los, C. J. Tucker, C. O. Justice, D. A. Dazlich, G. J. Collatz, and D. A. Randall (1996), A revised land surface parameterization (SiB2) for Atmospheric GCMs. Part II: The generation of global fields of terrestrial biophysical parameters from satellite data, *J. Clim.*, 9, 706–737.

Stamnes, K., S. C. Tsay, W. Wiscombe, and K. Jayaweera (1988), Numerically stable algorithm for discrete-ordinate-method radiative transfer in multiple scattering and emitting layered media, *Appl. Opt.*, 27, 2502–2509.

Tarpley, J. D. (1979), Estimating incident solar radiation at the surface from geostationary satellite data, *J. Appl. Meteorol.*, 18, 1172–1181.

Van Laake, P. E., and G. A. Sanchez-Azofeifa (2004), Simplified atmospheric radiative transfer modelling for estimating incident PAR using MODIS atmosphere products, *Remote Sens. Environ.*, 91, 98–113.

Van Laake, P. E., and G. A. Sanchez-Azofeifa (2005), Mapping PAR using MODIS atmosphere products, *Remote Sens. Environ.*, 94(4), 554–563.

———————————

H. Fang, S. Liang, and T. Zheng, Department of Geography, University of Maryland, College Park, MD 20742, USA. (sliang@geog.umd.edu)

R. Liu, Institute for Geographical Science and Natural Resources Research, Chinese Academy of Sciences, Beijing 100101, China.

S. Running, School of Forestry, University of Montana, Missoula, MT 59812, USA.

S.-C. Tsay, Climate and Radiation Branch, NASA/Goddard Space Flight Center, Greenbelt, MD 20771, USA.